N-terminal acetylation and the N-end rule pathway control degradation of the lipid droplet protein PLIN2

Received for publication, August 25, 2018, and in revised form, November 8, 2018 Published, Papers in Press, November 13, 2018, DOI 10.1074/jbc.RA118.005556

Kha The Nguyen, Chang-Seok Lee, Sang-Hyeon Mun, Nhung Thimy Truong, Sang Ki Park, and Cheol-Sang Hwang[1]

From the Department of Life Sciences, Pohang University of Science and Technology, Pohang, Gyeongbuk 37673, Republic of Korea

Edited by Ursula Jakob

Perilipin 2 (PLIN2) is a major lipid droplet (LD)-associated protein that regulates intracellular lipid homeostasis and LD formation. Under lipid-deprived conditions, the LD-unbound (free) form of PLIN2 is eliminated in the cytosol by an as yet unknown ubiquitin (Ub)-proteasome pathway that is associated with the N-terminal or near N-terminal residues of the protein. Here, using HeLa, HEK293T, and HepG2 human cell lines, cycloheximide chase, *in vivo* ubiquitylation, split-Ub yeast two-hybrid, and chemical cross-linking–based reciprocal co-immunoprecipitation assays, we found that TEB4 (MARCH6), an E3 Ub ligase and recognition component of the Ac/N-end rule pathway, directly targets the N-terminal acetyl moiety of Nα-terminally acetylated PLIN2 for its polyubiquitylation and degradation by the 26S proteasome. We also show that the TEB4-mediated Ac/N-end rule pathway reduces intracellular LD accumulation by degrading PLIN2. Collectively, these findings identify PLIN2 as a substrate of the Ac/N-end rule pathway and indicate a previously unappreciated role of the Ac/N-end rule pathway in LD metabolism.

Lipid droplets (LDs)[2] are the major lipid repository organelle and comprise a neutral lipid core enclosed by a phospholipid monolayer with its associated proteins. LD serves as a key depot for lipid metabolism and trafficking, protein quality control, nucleic acid binding, pathogen infection, etc. (1–3). The most abundant LD-coated proteins are the Perilipin (PLIN) family of proteins with a PAT domain (derived from the conserved region of Perilipin A, ADRP, and TIP47) at their N termini. Among the five members of the PLIN family, PLIN2 (ADRP or adipophilin) is universally expressed in nearly all tissues and plays a pivotal role in LD biogenesis, fatty acid uptake, and lipid accumulation (1–3). Hence, dysregulation of PLIN2 is associated with numerous metabolic diseases (cardiovascular diseases, hepatic steatosis, sarcopenia, obesity, and type 2 diabetes), cancers, inflammation, etc. (1). Crucially, the PLIN2 level is positively regulated by the abundance of intracellular LD and triacylglycerol content (2, 3). In particular, PLIN2 is stabilized upon the induction of LD formation by oleic acid treatment, whereas lipolytic stimuli, such as nutrient starvation without fatty acid supplementation, trigger degradation of LD-bound PLIN2 via chaperone-mediated autophagy (4) and that of LD-unbound free PLIN2 via the ubiquitin (Ub)-proteasome system (UPS) (5–7). Because degradation of LD-unbound free PLIN2 involves UPS in the cytosol, rapid deposition of PLIN2 onto the LD membrane is postulated to shield its degradation signals (degrons) from the UPS destruction machinery (2, 5, 8).

The N-end rule pathways in eukaryotes belong to the Ub-mediated proteolytic system, which recruits a cascade reaction of E1 (Ub-activating enzyme), E2 (Ub-conjugating enzyme), and E3 (Ub ligase) (9). A common feature of the eukaryotic N-end rule pathways is their ability to directly recognize the N-terminal degrons (N-degrons) of proteins, thereby polyubiquitylating them for degradation by 26S proteasome or lysosome (via autophagy) (9, 10). All N-degrons bear destabilizing N-terminal (Nt-) residues as a primary determinant, which may be conditionally activated upon their steric unshielding, proteolytic processing, or chemical modifications. The dedicated N-degron recognition component and its related proteolytic pathway are the N-recognin and the N-end rule pathway, respectively. Thus far, three N-end rule pathways have been elucidated in eukaryotes: Arg/N-, Pro/N-, and Ac/N-end rule pathways (11–13).

The Arg/N-end rule pathway is a conventional N-end rule pathway in which the UBR family E3 Ub ligases (as N-recognins) target unmodified destabilizing Nt-residues (Nt-Arg, Lys, His, Leu, Trp, Phe, Ile, Tyr, and Met-a hydrophobic residue (Met-Φ)). Nt-Asn, Gln, or Cys may be destabilized after preliminary modifications (Nt-deamidation, arginylation, and Cys-oxidation, respectively). Another N-end rule pathway is the Pro/N-end rule pathway in which a Pro/N-recognin GID4 E3 Ub ligase is recruited to target unmodified Nt-Pro residues for degradation of the protein (12, 14, 15).

Although the Arg/N- and Pro/N-end rule pathways target the unmodified free Nα-group of proteins, the Ac/N-end rule pathway targets acetylated Nα-termini, which are commonly found in eukaryotic proteins (~80% human proteins), for degradation. The degrons and recognition component of the

This work was supported by Samsung Science & Technology Foundation Grant SSTF-BA1401-17, National Research Foundation of Korea (NRF) grant funded by Korean Government(MSIP) Grant NRF-2017R1A5A1015366), the BK21 Plus Program, and the POSCO Green Science and Innovation Grant. The authors declare that they have no conflicts of interest with the contents of this article.

[1] To whom correspondence should be addressed. Tel.: 82-54-297-2352; Fax: 82-54-279-2291; E-mail: cshwang@postech.ac.kr.

[2] The abbreviations used are: LD, lipid droplet; PLIN2, perilipin2; Ub, ubiquitin; CHX, cycloheximide; Nt-acetylation, N-terminal acetylation; Nt-acetylase, N-terminal acetylase; ER, endoplasmic reticulum; Ac/N-end rule, N-terminal acetylation/N-end rule; UPS, ubiquitin-proteasome system; qPCR, quantitative PCR; DSP, dithiobis(succinimidyl propionate); HA, hemagglutinin; DMEM, Dulbecco's modified Eagle's medium; FBS, fetal bovine serum; PEI, polyethylenimine; IB, immunoblot; IP, immunoprecipitation.

Ac/N-end rule pathway are Ac/N-degrons and Ac/N-recognin, respectively (15, 16). The Ac/N-recognins are the endoplasmic reticulum (ER)/nuclear inner transmembrane protein Doa10 (TEB4 or MARCH6 in mammals) or the cytosolic/nuclear Not4 E3 Ub ligases (16–18). Because many eukaryotic proteins obtain an acetyl group at their N termini co-translationally and irreversibly, most proteins are postulated to retain Ac/N-degrons, which may be reversibly and conditionally exposed or operated (16). The conditionality of Ac/N-degrons and the Ac/N-end rule pathway is demonstrated by regulation of protein quality and subunit stoichiometry (through degradation of the Nt-acetylated subunits of COG; conserved subunits of the oligomeric Golgi complex; or Nt-acetylated Hcn1, a subunit of APC/C Ub ligase), blood pressure (through degradation of RGS2, a regulator of G-protein signaling), circadian rhythms (through degradation of arylalkylamine *N*-acetyltransferase (AANAT)), and plant stress response (through degradation of SNC1, a Nod-like receptor) (17–20).

Recently, Sato *et al.* (5) reported that C-terminally FLAG-tagged mouse PLIN2 is short-lived and is degraded by UPS, whereas the N-terminally FLAG-tagged PLIN2 is long-lived. Moreover, they found that mutations in alanine (Ala) residues at positions 2 or 3 to an Asp residue greatly stabilized mouse Plin2 in the cytosol. Given that mouse PLIN2 is Nα-terminally acetylated (Nt-acetylated), the free PLIN2 was thought to be degraded by the Ac/N-end rule pathway (5). However, the involvement of the Ac/N-end rule pathway in UPS-mediated degradation of PLIN2 has not been experimentally examined or demonstrated thus far.

Results

Nt-acetylation contributes to the degradation of human PLIN2

Mouse or human DNA-encoded WT PLIN2 begins with Met-Ala at the N terminus and is termed as [M]A-PLIN2. However, the Met residue of [M]A-PLIN2 is co-translationally removed by ribosome-bound methionine aminopeptidases (MetAPs) because the penultimate Ala residue is smaller than Val (Fig. 1*A*) (21). Thus, the bracket around the Nt-Met residue in [M]Z-PLIN2s (if Z is an Ala, Ser, Thr, Val, Cys, Gly, or Pro residue) indicates co-translational removal of the N-terminal Met. The resulting human PLIN2 exposes the Ala residue at position 2 as its N terminus, yielding an ~49-kDa A-PLIN2 protein. Notably, previous global proteomic analyses have revealed that human A-PLIN2 is N-terminally acetylated, as shown in mouse A-PLIN2 (5, 22, 23). N-terminal Ala, Ser, Thr, Val, Cys, Gly, or Val are primarily acetylated by NatA Nt-acetylase, which comprises the catalytic subunit NAA10, and the ancillary subunits NAA15 and HYPK in humans (24, 25).

PLIN2 is widely expressed in most mammalian cell lines and tissues in contrast to other PLINs whose expression are confined exclusively to adipocytes and steroidogenic cells (3). Thus, we directly examined whether Nt-acetylation of A-PLIN2 through NatA Nt-acetylase affects the stability of the protein, by first performing cycloheximide (CHX) chase assays in HeLa cells with transient expression of Nt-acetylatable and C-terminally doubly HA-tagged A-PLIN2 (A-PLIN2$_{ha2}$), followed by small-interfering RNA (siRNA)-based knockdown of

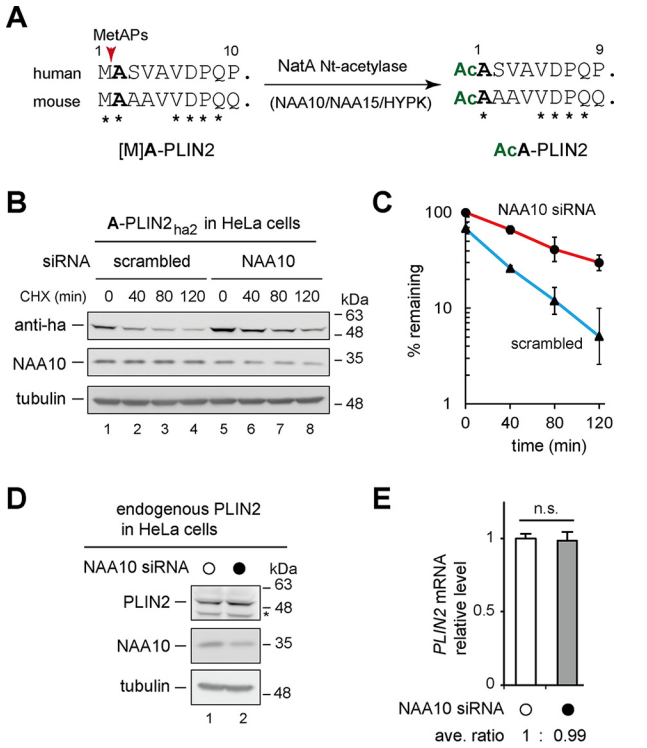

Figure 1. NatA Nt-acetylase contributes to degradation of PLIN2. *A,* human and mouse [M]A-PLINs are processed by MetAPs, and subsequently Nt-acetylated by the NatA complex (NAA10/NAA15/HPYK). *B,* CHX chases were carried out with A-PLIN2$_{ha2}$ exogenously expressed in HeLa cells that were subjected to siRNA for either a scrambled sequence (*lanes 1–4*) or *NAA10* (*lanes 5–8*). A-PLIN2$_{ha2}$, NAA10, or tubulin (a loading control) were detected via immunoblotting with anti-HA, anti-NAA10, or anti-tubulin antibodies, respectively. *C,* quantification of data in *A*. Data represent the mean ± S.E. of three independent experiments. *D,* expression levels of PLIN2 in HeLa cells that were subjected to siRNA either for a scrambled sequence (*lane 1*) or NAA10 (*lane 2*). *E,* relative levels of *PLIN2* mRNAs using RT-qPCR. The data represent the mean ± S.D. in triplicate for each sample. * denotes a nonspecific band.

NAA10, a catalytic subunit of the NatA Nt-acetylase. The CHX chase assay employs immunoblotting for measuring the *in vivo* time course turnover of a given protein in the presence of a translation inhibitor CHX. During the CHX chase assays in HeLa cells, with scrambled siRNA as a negative control, the exogenous A-PLIN2$_{ha2}$ was rapidly degraded, having a half-life of ~30 min. Conversely, siRNA-based knockdown of NAA10 markedly reduced degradation of A-PLIN2$_{ha2}$ to a half-life of ~70 min (Fig. 1, *B* and *C*). Moreover, the steady-state level of endogenous PLIN2 was increased by ~1.4-fold in HeLa cells upon NAA10 knockdown (Fig. 1*D*), although reverse transcription quantitative PCR (RT-qPCR) indicated no significant changes in the levels of *PLIN2* mRNA in HeLa cells subjected to siRNA for a scrambled sequence or *NAA10* (Fig. 1*E*).

TEB4 E3 Ub ligase recognizes PLIN2 for degradation via UPS

Our previous study identified the ER membrane-spanning E3 Ub ligase TEB4 (MARCH6, the counterpart of *Saccharomyces cerevisiae* Doa10) as an Ac/N-recognin of the mammalian Ac/N-end rule pathway (18). Based on the above observation that NatA-mediated Nt-acetylation of A-PLIN2 markedly contributed to the stability of the protein (Fig. 1*A*), we demonstrated that TEB4 acts as the Ac/N-recognin for degradation of human PLIN2 (see Figs. 2 to 5 for details).

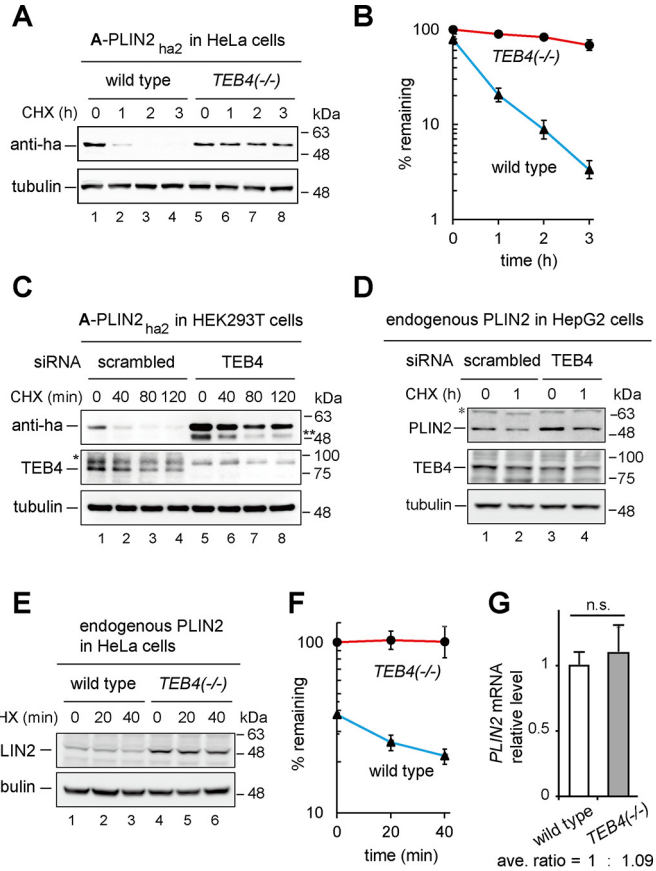

Figure 2. A-PLIN2 is stabilized in the absence of TEB4. *A,* CHX chases for 0, 1, 2, and 3 h with exogenous A-PLIN2$_{ha2}$ in WT (*lanes 1–4*) and *TEB4*$^{-/-}$ KO (*lanes 5–8*) HeLa cells. *B,* quantification of data in *A*. Data represent the mean ± S.E. of three independent experiments. *C,* CHX chases for 0, 20, 80, and 120 min with exogenous A-PLIN2$_{ha2}$ in HEK293T cells that were subjected to siRNA for a scrambled sequence (*lanes 1–4*) or TEB4 (*lanes 5–8*). *D,* same as in *C* but for 0 and 1 h with endogenous PLIN2 in HepG2 cells. *E,* same as in *A* but for 0, 20, and 40 min with endogenous PLIN2. *F,* quantification of data in *E*. Data represent the mean ± S.E. of three independent experiments. *G,* quantification of the relative levels of *PLIN2* mRNA using RT-qPCR. The data represent the mean ± S.D. from RT-qPCR assays in triplicate for each sample. * and ** denote nonspecific bands and a cleaved product of A-PLIN2$_{ha2}$, respectively.

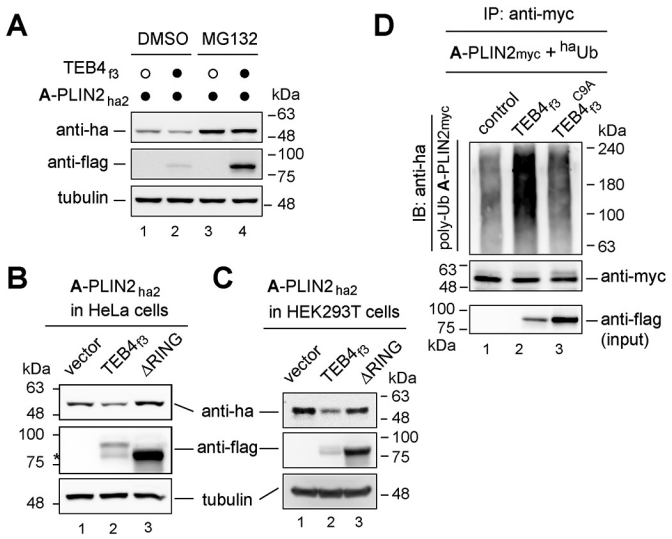

Figure 3. TEB4 mediates the polyubiquitylation of A-PLIN2$_{ha2}$ for proteasomal degradation. *A,* A-PLIN2$_{ha2}$ in HeLa cells with or without TEB4$_{f3}$ in either the presence or absence of the proteasome inhibitor MG132. *B,* A-PLIN2$_{ha2}$ in HeLa cells transiently overexpressing TEB4$_{f3}$ (*lane 2*), and TEB4$_{f3}^{\Delta RING}$, a truncated mutant lacking the catalytic RING domain of TEB4 E3 Ub ligase (*lane 3*). *C,* same as in *B* but with HEK293T cells. *D, in vivo* ubiquitylation assay of A-PLIN2$_{ha2}$ in HeLa cells transiently co-expressing ^{ha}Ub and A-PLIN2$_{myc}$ together with either the WT TEB4 (*lane 2*), or the catalytically inactive mutant, TEB4^{C9A} (*lane 3*). Polyubiquitylated A-PLIN2$_{ha2}$ were detected by immunoblotting with anti-HA antibody (*upper panel*) after co-immunoprecipitation of A-PLIN2$_{myc}$ with anti-myc antibody (*middle panel*). * denotes a cleaved product of TEB4$_{f3}$.

First, exogenous A-PLIN2$_{ha2}$ was short-lived in WT HeLa cells, having a half-life of ~30 min, but was strongly stabilized in CRISPR/Cas9-based *TEB4*$^{-/-}$ knockout (KO) cells, in which its half-life was extended to ~330 min (Fig. 2, *A* and *B*). Notably, the TEB4-dependent degradation patterns of exogenous A-PLIN2$_{ha2}$ were largely retained in WT and TEB4-knockdown HEK293T cells as well (Fig. 2*C*). In agreement with observations of exogenous A-PLIN2$_{ha2}$, endogenous A-PLIN2 was also markedly stabilized in *TEB4*$^{-/-}$ HeLa cells, although that of in WT HeLa cells was barely detectable even before the CHX chases and was also unstable with the half-life of ~30 min (Fig. 2, *E* and *F*). RT-qPCR revealed almost no significant alterations in levels of *PLIN2* mRNA between WT and *TEB4*$^{-/-}$ KO HeLa cells (Fig. 2*G*), indicating that the observed up-regulation in the level of endogenous A-PLIN2 in *Teb4*$^{-/-}$ KO cells is most likely due to changes in the rate of its initial degradation, particularly considering that multiple lines of evidence suggest substantial co-translational proteolysis of newly synthesized proteins (26–28). Furthermore, CHX chase showed that TEB4 knockdown resulted in a significant stabilization of endogenous PLIN2 in HepG2 cells as well (Fig. 2*D*).

Second, the level of transiently expressed A-PLIN2$_{ha2}$ was substantially increased following the application of the proteasome inhibitor MG132, whereas co-expression of C-terminally triple FLAG-tagged TEB4 (TEB4$_{f3}$) and A-PLIN2$_{ha2}$ in HeLa cells diminished the level of A-PLIN2$_{ha2}$ (Fig. 3*A*).

Third, the level of A-PLIN2$_{ha2}$ was not down-regulated when TEB4$_{f3}^{\Delta RING}$, a truncated mutant lacking the catalytic RING domain of an Ub ligase, was co-expressed compared with that when WT TEB4$_{f3}$ was co-expressed in HeLa cells (Fig. 3*B*). Noteworthy, the level of catalytically inactive TEB4$_{f3}^{\Delta RING}$ was greatly up-regulated in agreement with the previous finding that TEB4 targets itself for degradation (29). Importantly, almost the same results were obtained in HEK293T cells, suggesting that TEB4-mediated down-regulation of A-PLIN2 is most likely conserved in different cell lines (Fig. 3*C*).

Fourth, the *in vivo* ubiquitylation assay in HeLa cells transiently expressing C-terminally myc-tagged A-PLIN2 (A-PLIN2$_{myc}$) in conjunction with N-terminally HA-tagged Ub (^{ha}Ub) showed that level of polyubiquitylated A-PLIN2$_{myc}$ was markedly increased by co-expression of TEB4$_{f3}$, but not by that of the TEB4$^{C9A}_{f3}$, a missense mutant that is catalytically inactive as an Ub ligase (Fig. 3*D*).

Last, the modified split-Ub assay and chemical cross-linking–based reciprocal co-immunoprecipitation assays (see "Experimental procedures") demonstrated physical binding of TEB4 to A-PLIN2 (Fig. 4). Together, these results indicate that TEB4 directly interacts with A-PLIN2 for polyubiquitin-mediated and proteasome-dependent degradation.

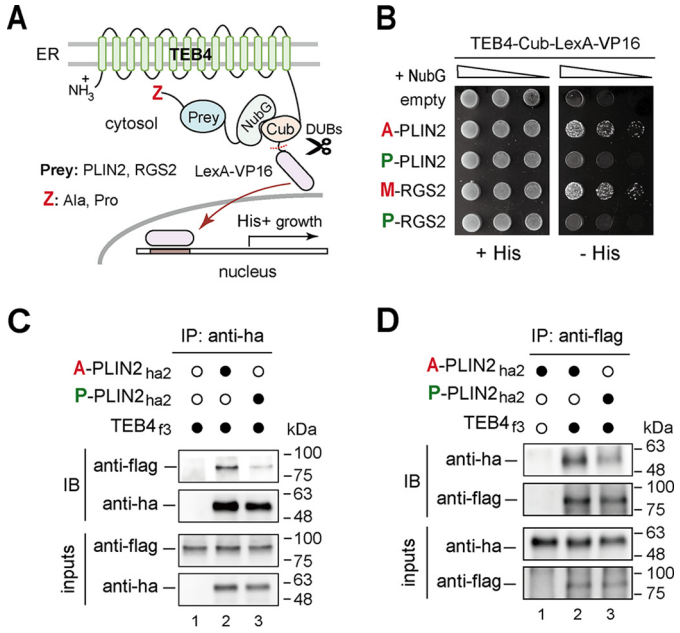

Figure 4. TEB4 interacts Nt-acetylatable A-PLIN2 more preferentially than otherwise identical but nonacetylatable P-PLIN2. *A,* depicted is a schematic representation of the split-Ub assay used in the present study. The ER transmembrane TEB4 is directly linked to Cub-LexA-VP16. [M]A-PLIN2, [M]P-PLIN2, M-RGS2, or [M]P-RGS2 were each fused to the N-terminal half of the Ub mutant (NubG). *B,* an *in vivo* interaction between TEB4 and PLIN2 or RGS2 leads to a positive assay using the ER transmembrane full-length TEB4 and [M]A-PLIN2 *versus* [M]P-PLIN2, or M-RGS2 *versus* [M]P-RGS2. [M] denotes N-terminal Met before its co-translational cleavage. Nt-acetylatable M-RGS2 and non-Nt-acetylatable P-RGS2 (derived from [M]P-RGS2 after co-translational removal of Nt-Met) were used as a positive or negative control for this assay, respectively. *C,* HeLa cells co-expressing $TEB4_{f3}$ and either vector only (*lane 1*), $A\text{-}PLIN2_{ha2}$ (*lane 2*), or $P\text{-}PLIN2_{ha2}$ (*lane 3*) were fixed with a membrane-permeable chemical cross-linker, DSP, followed by immunoprecipitations with anti-HA, cross-linking reversal, SDS-PAGE fractionation, and immunoblotting with anti-FLAG or anti-HA antibodies. *D,* same as in *C,* but $A\text{-}PLIN2_{ha2}$ alone without $TEB4_{f3}$ in *lane 1*, and immunoprecipitations with anti-FLAG antibody.

TEB4 interacts preferentially with Nt-acetylatable PLIN2 variants

To further verify specific recognition of an Ac/N-degron of PLIN2 by TEB4, we slightly modified the split-Ub assay (30, 31) using the ER membrane-embedded TEB4 as a bait protein and Nt-acetylatable A-PLIN2 (bearing an Ala residue at the N terminus) or non-Nt-acetylatable P-PLIN2 (bearing a Pro residue at the N terminus after co-translational Nt-Met cleavage of [M]P-PLIN2) as prey proteins (Fig. 4*A*) because global proteomic analyses demonstrate that the Nt-Pro residue of cellular proteins is almost never Nt-acetylated (24, 32, 33). In this split-Ub assay, the C-terminal half of Ub (Cub) followed by a LexA-VP16 transcription factor were directly anchored to the cytosol-faced C terminus of the 14-transmembrane TEB4, yielding TEB4-Cub-LexA-VP16. Conversely, Nt-acetylatable A-PLIN2 and nonacetylatable P-PLIN2 were each fused to a mutant variant of the N-terminal half of Ub (NubG), producing A-PLIN2-NubG and P-PLIN2-NubG, respectively. If TEB4 and PLIN2 interact with each other, Cub and NubG create a quasi-native Ub moiety, which is, in turn, recognized by yeast deubiquitylases. Consequently, deubiquitylases process the nascent polypeptide downstream from Cub, liberating the LexA-VP16 transcription factor from the ER membrane, and subsequently induce the Lex-responsive reporter genes (Fig. 4*A*). Based on our previous finding that TEB4 specifically interacts with Nt-acetylatable WT M-RGS2 (bearing a Met residue at the N terminus) but not with non-Nt-acetylatable P-RGS2 (bearing a Pro residue at the N terminus after co-translational Nt-Met cleavage of [M]P-RGS2) (18), we also constructed M-RGS2-NubG and P-RGS2-NubG reporters as TEB4-binding positive and negative controls, respectively (Fig. 4*A*). Co-expression of TEB4 and Nt-acetylatable M-RGS2 or A-PLIN2 produced the interaction-positive His+ readout (growth phenotype) reproducibly on selective histidine-lacking media. In contrast, no His^+ cells were observed with non-Nt-acetylatable P-PLIN2 as well as with negative controls (vector only or non-Nt-acetylatable P-RGS2). Thus, this split-Ub–based analysis indicated that TEB4 interacted with Nt-acetylated Ac-A-PLIN2 or Ac-M-RGS2, but not significantly with otherwise identical, but non-Nt-acetylated, P-PLIN2 or P-RGS2 (Fig. 4*B*). Furthermore, chemical cross-linking and reciprocal co-immunoprecipitation assays revealed that TEB4 bound more strongly to Nt-acetylatable $A\text{-}PLIN2_{ha2}$ than to non-Nt-acetylatable $P\text{-}PLIN2_{ha2}$ in HeLa cells (Fig. 4, *C* and *D*). Nonetheless, the marginal, but still detectable, interaction of TEB4 with non-Nt-acetylatable P-PLIN2 suggested that TEB4 recognized the internal degron of the protein to a lesser extent (Fig. 4, *C* and *D*).

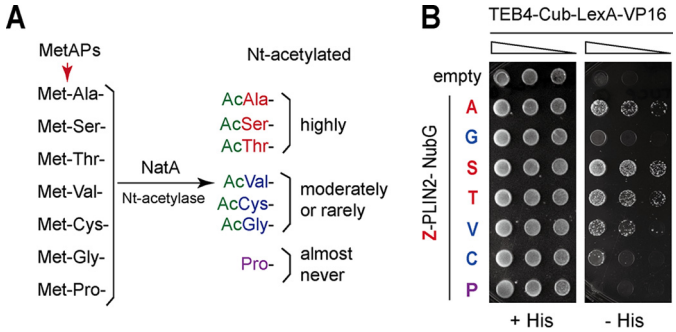

Figure 5. Substrate specificity of NatA Nt-acetylase. *A,* depicted substrate specificity of the NatA complex. NatA acetylates N-terminal Ser, Ala, Thr, Val, Cys, or Gly, thus modifying 30–40% of proteins from the total human proteome. Specially, Ser and Ala are highly Nt-acetylated, Thr and Val moderately, Cys and Gly rarely, and Pro almost never. *Ac* indicates "the Nα-terminal acetyl moiety." *B,* split-Ub assays using TEB4 and [M]Z-PLIN2 with Ser, Ala, Thr, Val, Cys, or Gly at position 2. Note that the binding of TEB4 to PLIN2 correlates with the Nt-acetylation tendency (extent) of NatA substrates.

Given the recognition of the Ac/N-degron of Nt-acetylated A-PLIN2 by TEB4, we further aimed to compare interactions between TEB4 and Z-PLIN2s bearing varied Nt-residues that are targeted by NatA Nt-acetylase (Z = Ala, Gly, Ser, Thr, Val, Cys, or Pro) (Fig. 5*A*). The Z-PLIN2s are produced after co-translational Nt-Met removal of human DNA-encoded [M]Z-PLIN2s by MetAPs. In this split-Ub assay, *in vivo* levels of His-3 were largely correlated with rates of *S. cerevisiae* growth in histidine-lacking media, thus making it possible to analyze the binding capacity of TEB4 to Z-PLIN2s by comparing the growth of serially diluted yeast cells on selective plates without histidine. These split-Ub-based growth assays showed that TEB4 interacted strongly with A-PLIN2, S-PLIN2, and T-PLIN2, to a lesser extent with V-PLIN2, and very slightly with C-PLIN2 or G-PLIN2, but showed almost no interaction with P-PLIN2 (Fig. 5*B*). Strengths of the interactions estimated

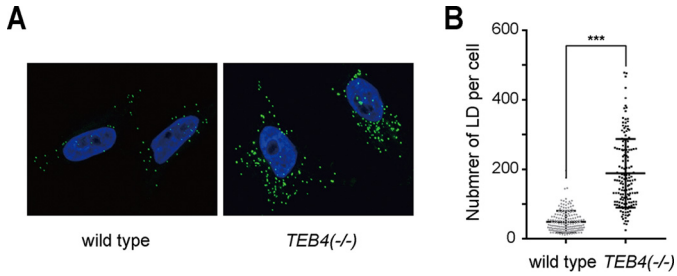

Figure 6. Ablation of TEB4 increases LD contents. *A*, the number of LDs was calculated using confocal fluorescent microscopy after staining WT and *TEB4*$^{-/-}$ KO HeLa cells with BODIPY 493/503. *B*, quantification of *A* was statistically significant and displayed as the column scatter plot of all individual cells. The unpaired Student's *t* test yielded a *p* value < 0.001 (***).

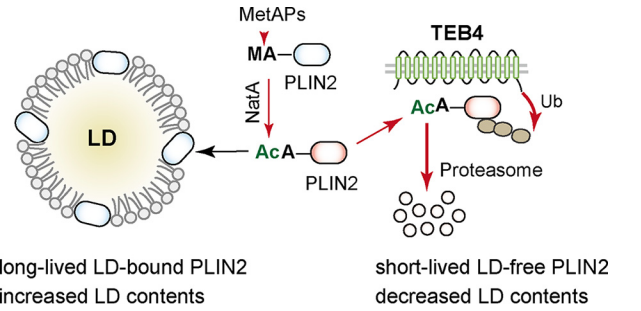

Figure 7. Model for PLIN2 degradation by the Ac/N-end rule pathway. Under lipid-rich conditions, Nt-acetylated PLIN2 is attached to LD for stabilization. In contrast, under lipid-deprived conditions, Nt-acetylated A-PLIN2 is recognized by TEB4 E3 Ub ligase for polyubiquitin-mediated degradation by the 26S proteasome.

from these split-Ub–based growth assays are in the following order: Nt-Ser > Ala ≈ Thr > Val > Cys > Gly > Pro. These interaction results of TEB4 with Z-PLIN2s largely, but not entirely, corresponded with the Nt-acetylation tendency of *S. cerevisiae* proteins by NatA Nt-acetylase; *i.e.* Ser and Ala are highly Nt-acetylated, Thr and Val are moderately Nt-acetylated, Cys and Gly are rarely Nt-acetylated, and Pro is almost never Nt-acetylated (Fig. 5*A*) (14, 24, 25).

TEB4 controls LD abundance

Multiple lines of evidence show that overexpression of PLIN2 promotes LD abundance, whereas its depletion down-regulates LD formation in various types of cells (3, 34–36). Accordingly, we examined whether TEB4 modulates intracellular LD contents through PLIN2 degradation. To directly stain intracellular LDs, WT and *TEB4*$^{-/-}$ KO HeLa cells were treated with the hydrophobic fluorescent dye BODIPY 493/503. Fluorescent microscopy analysis revealed that the number of intracellular LDs increased by ~3-fold in *TEB4*$^{-/-}$ KO HeLa cells compared with that in WT cells, indicating that ablation of TEB4 leads to substantial LD accumulation through the up-regulation of PLIN2 (Fig. 6).

Discussion

A major LD-associated protein, PLIN2, is ubiquitously expressed in different types of cells, and plays key roles in LD formation and lipid storage. LD-anchored PLIN2 is eliminated via the chaperone-mediated autophagy pathway, thus, accelerating intracellular lipolysis (4). However, free PLIN2 is subjected readily to the UPS-mediated degradation in the cytosol under lipid-deprived conditions (1, 3, 5). Notably, PLIN2 degradation is affected drastically by mutations in its conserved N terminus or near N-terminal residues (5). Yet, little is known about the underlying mechanism of how the UPS-dependent PLIN2 proteolysis occurs (2, 5).

The present study demonstrated that the knockdown of NAA10, a catalytic subunit of the NatA complex, resulted in significant stabilization of A-PLIN2 (Fig. 1). In addition, loss of TEB4, a mammalian Ac/N-recognin, substantially stabilized the levels of exogenous and endogenous PLIN2 (Fig. 2). Specifically, TEB4 mediated the polyubiquitylation of Nt-acetylatable A-PLIN2 for degradation by 26S proteasomes (Fig. 3). Furthermore, this study showed that TEB4 interacted specifically with Nt-acetylatable A-PLIN2, but not with non-Nt-acetylatable P-PLIN2 (Fig. 4). Crucially, the Nt-acetylation-dependent interaction between TEB4 and PLIN2 was also verified by the split-Ub assays using PLIN2 derivatives with varied Nt-acetylatable or non-Nt-acetylatable residues at their N termini (Fig. 5). Strikingly, the ablation of TEB4 increased cellular LD contents by ~3-fold, which is in agreement with the strong up-regulation of PLIN2 levels observed in *TEB4*$^{-/-}$ KO cells compared with those of WT HeLa cells (Figs. 2*E* and 6), highlighting the previously unknown function of TEB4 in LD homeostasis. Altogether, we discovered that the Ac/N-end rule pathway destroys Nt-acetylated PLIN2 in the cytosol, thus, leading to the down-regulation of intracellular LD contents (Fig. 7). In addition, it is noteworthy that A-PLIN2 is the first example of a NatA-dependent substrate of the Ac/N-end rule pathway to be identified in mammals, although the NatA complex acetylates 30–40% of the N termini in the human proteome (12, 27).

Earlier studies have demonstrated that PLIN2 is long-lived when it is associated with the LD monolayer by replacement of another LD-associated protein, PLIN1, or when the flux of intracellular lipids is increased (2, 5, 7, 37). Under lipid-rich conditions, PLIN2 contacts directly with neutral lipids and retains a SNARE complex protein, SNAP23, on the LD via their augmented interaction (38). Considering the degradation of free PLIN2 by the UPS in the cytosol, such lipid or protein bindings most likely induce its conformational change and, subsequently, shield the Ac/N-degron, thus protecting the PLIN2 protein from destruction by the TEB4-mediated Ac/N-end rule pathway, in agreement with the conditionality of Ac/N-degrons demonstrated in our previous works (12, 17, 18). Another plausible explanation for the stabilization of PLIN2 on LD most likely stems from the spatial segregation between LD-anchored PLIN2 and ER-embedded TEB4, which would prevent the interaction of the Ac/N-degron of PLIN2 with TEB4 E3 Ub ligase. Nonetheless, we cannot exclude the possibility that TEB4 is still in proximity to the PLIN2 protein, and targets it for degradation while LD is budding from ER membrane, as Doa10 (a counterpart of TEB4 in *S. cerevisiae*) regulates the abundance of the LD-associated proteins during LD biogenesis from the ER (39).

A recent systemic survey of the yeast N-terminome using multiplexed protein stability profiling argued that Nt-acetylation contributes to the substrate recognition of Doa10 (a yeast homolog of TEB4) by elevating the overall hydrophobicity of

the N terminus rather than by creating a specific degron (40). Although the possibility is not mutually exclusive, our split-Ub analyses indicate that TEB4 specifically recognizes the Nt-acetyl moiety of PLIN2, regardless of the hydrophobicity rendered by the acetylated residues (Figs. 4 and 5). Specially, S-PLIN2 (having a hydrophilic Ser N terminus) interacted similarly or more strongly with TEB4 than A-PLIN2 or V-PLIN2 (having a hydrophobic Ala or Val N terminus, respectively) (Fig. 5). Moreover, global N-terminome analyses reveal that Ala, Ser, or Thr N termini of proteomes are more acetylated than Val or Cys N termini (41, 42). Complying with the varying efficacy of Nt-acetylation depending upon the species of Nt-residues, the split-Ub results also demonstrate that TEB4 interacts preferentially with A-PLIN2, S-PLIN2, or T-PLIN2 bearing Nt-acetylation-prone Nt-residues than otherwise identical, but rarely or almost never Nt-acetylated V-PLIN2, C-PLIN2, G-PLIN2, or P-PLIN2 (Fig. 5) (22, 30). Future detailed biochemical and structural analyses will provide a more complete understanding of how TEB4 specifically recognizes the Nt-acetyl tag of Nt-acetylated proteins.

With respect to LD and lipid metabolism, TEB4 mediates degradation of not only PLIN2, but also squalene monooxygenase, a rate-limiting enzyme in cholesterol synthesis (43, 44, 46). In addition, Doa10 (a yeast homolog of mammalian TEB4) is shown to spatially target LD proteins that are integrated into the ER membrane (39). Hence, our present finding indicates that TEB4 acts as a key regulator of lipid homeostasis and LD metabolism by mediating degradation of PLIN2 via the Ac/N-end rule pathway. Importantly, deregulation of PLIN2 expression is associated with the emergence of various age-related metabolic diseases, cancers, and inflammation (1). Therefore, further detailed analysis of the TEB4-mediated degradation of PLIN2 by the Ac/N-end rule pathway will provide new therapeutic targets to treat such intractable diseases.

Table 1
Plasmids used in this study

Plasmid	Description	Source
pCH60	pcDNA3.1 neo (+)	Hwang's lab collection
pCH61	pcDNA3.1 (+) with ha_2	Hwang's lab collection
pCH341	pDHB1-OST4-Cub-LexA-VP16	31
pCH346	pDL2-Alg5	31
pCH836	TEB4 in pDHB1	This study
pCH879	$TEB4_{f3}$ in pcDNA3.1	18
pCH880	$TEB4_{f3}$ C9A in pcDNA3.1	18
pCH4502	pX330-U6-Chimeric_BB-CBh-hSpCas9	49
pCH6513	pCAG-EGxxFP	45
pCH6514	TEB4 fragment in pCAG-EGxxFP	This study
pCH6515	gRNA targeting Exon2 TEB4 in pCH4502	This study
pCH6567	MA-$Plin2_{ha2}$ in pcDNA3.1 (+)	This study
pCH6571	MA-$Plin2_{myc}$ in pcDNA3.1 (+)	This study
pCH7059	MA-Plin2 in pDL2	This study
pCH7060	MP-Plin2 in pDL2	This study
pCH7061	MG-Plin2 in pDL2	This study
pCH7062	MV-Plin2 in pDL2	This study
pCH7063	MS-Plin2 in pDL2	This study
pCH7064	MT-Plin2 in pDL2	This study
pCH7065	MC-Plin2 in pDL2	This study

Table 2
Some PCR primers used in this study

Name	Primer sequences
OCH4295	5′-GCCTCTAGAATGGACACCGCGGAGGAAGAC
OCH4296	5′-GATGGCCGAGGCGGCCAGTTCTTGGGATGACTGTGGAGGTGG
OCH4317	5′-GCCACTAGT ATGGCATCCGTTGCAGTT-3′
OCH6007	5′-CACCGTGTAGAGTGTGTCGGTCAGA-3′
OCH6008	5′-AAACTCTGACCGACACACTCTACAC-3′
OCH6531	5′-CCTCGCCTTTGCCGATCC-3′
OCH6532	5′-CTCGTCGCCCACATAGGAAT-3′
OCH6746	5′-CTTGGTACCATGGCATCCGTTGCAGTTGATCC-3′
OCH6747	5′-AACCTCGAGATGAGTTTTATGCTCAGATCGCTGGGT-3′
OCH6749	5′-CTTGGTACCATGCCATCCGTTGCAGTTGATCC-3′
OCH6789	5′-GGTGAATTCATGGCATCCGTTGCAGTTGATCC-3′
OCH8054	5′-GGCAGAGAACGGTGTGAAGA-3′
OCH8055	5′-TGTCTAGCCCCTTACAGGCA-3′
OCH8058	5′-CTTGGTACCATGAGTTTTATGCTCAGATCGCTGGGT-3′
OCH7131	5′-AATACTAGTATGGCATCCGTTGCAGTTGATC-3′
OCH7132	5′-AATATCGATATGAGTTTTATGCTCAGATCGCTGGG-3′
OCH7171	5′-AATACTAGTATGGGCTCCGTTGCAGTTGATCC-3′
OCH7172	5′-AATACTAGTATGGTGTCCGTTGCAGTTGATCC-3′
OCH7173	5′-AATACTAGTATGTCCTCCGTTGCAGTTGATCC-3′
OCH7174	5′-AATACTAGTATGACCTCCGTTGCAGTTGATCC-3′
OCH7175	5′-AATACTAGTATGTGCTCCGTTGCAGTTGATCC-3′

Experimental procedures

Miscellaneous materials and antibodies

Bovine serum albumin (BSA) (A9647), cycloheximide (C7698), phenylmethanesulfonyl fluoride (93482), cOmplete EDTA-free protease inhibitor mixture (11873580001) were purchased from Sigma. 4,4-Difluoro-1,3,5,7,8-pentamethyl-4-bora-3a,4a-diaza-*s*-indacene (BODIPY 493/503) (D3922) and dithiobis(succinimidyl propionate) (DSP) Lomant's reagent (22585) were purchased from Thermo Fisher Scientific, and MG132 (474790) from Calbiochem. Antibodies used in the present study for immunoblotting (IB) and/or immunoprecipitation (IP): anti-FLAG (Sigma, F7425 or F1804) (1:2,000 (IB), 1:1000 (IP)), anti-hemagglutinin (HA) tag (Sigma, H9658 or H6908) (1:2,000 (IB), 1:1,1000 (IP)), anti-PLIN2 (Abcam, ab78920) (1:1,1000), anti-tubulin (Sigma, T5168) (1:2,000), anti-TEB4 (Bethyl Laboratories, A304-171A) (1:1,000), anti-ARD1 (Santa Cruz Technology, sc-33256) (1:500), anti-squalene monooxygenase (SQLE) (Proteintech, 12544-1-AP) (1:500), and anti-myc tag (Genetex, GTX29106; Sigma, M4439) (1:2,000 (IB), 1:1,000 (IP)). Horseradish peroxidase-conjugated secondary antibodies used for immunoblotting: goat anti-rabbit IgG (Bio-Rad, 170-6515) (1:5,000) and anti-mouse IgG (Bio-Rad, 170-6516) (1:5,000). Dynabeads Protein A and G (Thermo Fisher Scientific, 10001D and 10003D) were used for immunoprecipitation experiments.

Construction of plasmids and primers

The plasmids and PCR primers used in the present study are listed in Tables 1 and 2, respectively. *Pfu-X* DNA polymerase (SolGent, South Korea) was used to perform PCR for cloning. *Escherichia coli* DH5α was primarily employed for the cloning and maintenance of plasmids. To construct the pCH6567 plasmid that expressed $PLIN2_{ha2}$ from pCDNA3.1(+), the primer pair OCH6746/OCH6747 was used to amplify *PLIN2* ORF from total HeLa cell cDNA. Total HeLa cell cDNA was synthesized from total RNAs extracted from HeLa cells using an RNeasy mini kit (Qiagen, 74106) and reverse-transcribed into cDNA using a TOPscript^{TM} cDNA synthesis kit (Enzynomics, EZ005S, South Korea). The resulting PCR product was digested with KpnI/XhoI, and ligated into the KpnI/XhoI-cut pCH61. To create the pCH6571 plasmid that expressed the C-terminally myc-tagged PLIN2 ($PLIN2_{myc}$), the *PLIN2* ORF was amplified using primer pair OCH6789/OCH8058 from pCH6567, digested with EcoRI/KpnI, and ligated into EcoRI/KpnI-cut pCH6567.

For the split-Ub assays, the primer pair OCH4295/OCH4296 was used to amplify the *TEB4* ORF from pCH879. The resulting DNA fragment was digested with XbaI and SfiI, and ligated into XbaI/SfiI-cut pCH341, creating pCH4200 (for the expression of TEB4 as a bait). In addition, the *PLIN2* ORF was PCR-amplified from pCH6567 using primer pair OCH4317/OCH7132 (MA-*PLIN2*), digested with SpeI/ClaI, and cloned into SpeI/ClaI-cut pCH346 to create pCH7059. The rest of the *PLIN2* mutants were constructed from the pCH7059 template using primer pairs OCH7131/OCH7132, OCH7171/OCH7132, OCH7172/OCH7132, OCH7173/OCH7132, OCH7174/OCH7132, and OCH7175/OCH7132 to amplify the mutant constructs. All were subsequently digested with SpeI/ClaI, and ligated into SpeI/ClaI-cut pCH346 to create pCH7060 (expressed [M]P-PLIN2), pCH7061 (expressed [M]G-PLIN2), pCH7062 (expressed [M]V-PLIN2), pCH7063 (expressed [M]S-PLIN2), pCH7064 (expressed [M]T-PLIN2), and pCH7065 (expressed [M]C-PLIN2), respectively. Plasmids harboring the *PLIN2* gene and its variants were used to express PLIN2 as preys in the split-Ub assay.

Yeast strains, media, genetic techniques, and split-Ub assays

Standard yeast media, as well as genetic and transformation techniques, were adapted for the construction of *S. cerevisiae* strains (47). The yeast culture media included YPD (1% yeast extract, 2% peptone, 2% glucose) and synthetic complete (SC) media (6.7% ammonium sulfate with yeast nitrogen base, 2% glucose, and a drop-out mixture of nutrients necessitated for a given auxotrophic yeast strains).

To examine the interaction between TEB4 and PLIN2, the split-Ub assay was slightly modified as follows (31): to exclude the possibility of PLIN2 degradation or the degradation of its derivatives by two major branches of the N-end rule pathway, the *S. cerevisiae* strain CHY713 (*ubr1*Δ*::kanMX6 doa10*Δ*::NatMX4* in NMY51), which lacks the sole Arg/N-recognin Ubr1 and ER-embedded Ac/N-recognin Doa10, was created using a PCR-mediated gene-targeting technique and the kanMX6 and natNT2 module in the split yeast two-hybrid strain NMY51 (31, 48). TEB4-bearing bait vector and PLIN2- or RGS2-bearing prey vectors were co-transformed into *S. cerevisiae* strain CHY713 through the conventional lithium-acetate transformation technique. Single colonies of transformants were cultured in SC(-Leu/-Trp) media to A_{600} of ~1.0. The same volumes of the resulting cultures were diluted using a 4-fold serial dilution, spotted on either SC(-Trp/-Leu) or SC(-Trp/-Leu/-His) plates, and then incubated at 30 °C for 2–3 days.

Cell culture, transfection, RNAi, and CRISPR/Cas9 gene knockout

Human HeLa, HEK293T, or HepG2 cells were cultured in Dulbecco's modified Eagle's medium (DMEM) (Welgene, LM001–05) containing 10% fetal bovine serum (FBS) (HyClone, SH30919.03) and penicillin (100 units/ml)/streptomycin (100 μg/ml) (HyClone, SV30010) at 37 °C in a 5% CO_2 incubator. DNA-plasmid transfections were performed using polyethylenimine (PEI) (1 mg/ml of stock solution prepared in distilled water at pH 7.0).

For siRNA-based knockdowns, HeLa, HEK293T, or HepG2 cells were seeded at 1×10^5 cells per well in 12-well cell culture plates (SPL Life Sciences, South Korea) with DMEM supplemented with 10% FBS. After a 24-h culture, the HeLa cells were transfected with 100 nM *NAA10*, *TEB4*, or nontargeting scrambled siRNAs (Santa Cruz Biotechnology, sc-44713, sc-91789, and sc-37007, respectively) using Lipofectamine 2000 or RNAiMax (Thermo Fisher, 11668019 or 13778150) according to the manufacturer's protocols.

To knockout *TEB4* in HeLa cells using the CRISPR/Cas9 system, a gRNA targeting *TEB4* exon2 (near a start codon) was designed using the online CRISPR design tool (http://crispr.mit.edu/).[3] The gRNA sequence (5′-TGTAGAGTGTGTCGGTCAGA-3′) followed by the protospacer adjacent motif was cloned into a pX330 plasmid (Addgene, 42230) under the U6 promoter. To confirm the gene-targeting efficiency of the gRNA, an ~1,000 bp DNA fragment covering the gRNA sequence was PCR amplified from the total HeLa cell cDNAs using primer pair OCH6525/OCH6526. The PCR product was digested with BamHI/EcoRI and ligated into BamHI/EcoRI-cut pCAG-EGxxFP, yielding pCH6514. To produce pCH6515 containing the gRNA sequence in the pX330 plasmid, primers OCH6007/OCH6008 were phosphorylated and annealed, and then cloned into BbsI-digested pX330. The PEI transfection method was used to co-transfect pCH6514 and pCH6515 into HeLa cells. After a 48-h culture, the transfected cells were trypsinized and appropriately diluted to generate single colonies. Thereafter, enhanced green fluorescent protein-expressing cells were selected, and the $TEB4^{-/-}$ knockout was verified via immunoblotting with anti-TEB4 antibodies and subsequent genomic DNA sequencing.

CHX-chase assays

CHX chases with HeLa cells were performed largely as previously described (18). Briefly, HeLa cells were diluted with DMEM and 10% FBS on day 1 to yield 1×10^5 cells/well in 12-well culture plates and, then, transfected with 0.5 μg of pCH6567 and 5 μl of PEI (1 mg/ml). After a 48-h incubation at 37 °C in a 5% CO_2 incubator, the cells were treated with CHX at a final concentration of 100 μg/ml, collected, and harvested with the RIPA buffer at the given time points (Thermo Fisher Scientific, 89900). After incubating on ice for 30 min, the cell lysates were centrifuged at 17,500 × *g* for 15 min at 4 °C to remove cell debris, and the supernatants were collected for protein quantification using the Bradford assay (Bio-Rad, 5000006), according to the manufacturer's protocol. Equal amounts of protein from cell lysates were mixed with Laemmli sample buffer and separated via Tris glycine, SDS-10% PAGE, followed by immunoblotting with anti-HA or anti-tubulin antibodies. Immunoblotting with anti-tubulin antibodies was employed as a loading control for the sample proteins. Immunoblots were developed with an ECL Plus Western blotting Detection System and analyzed with LAS-4000 (GE Healthcare). ImageJ software was used to perform the quantification of immunoblotting density. Error bars represente the

[3] Please note that the JBC is not responsible for the long-term archiving and maintenance of this site or any other third party hosted site.

mean ± S.E., which was calculated from three independent experiments.

RNA isolation and quantitative PCR

Total RNA were extracted from WT and *TEB4*$^{-/-}$ KO HeLa cells using an RNeasy mini kit (Qiagen, 74104) according to the manufacturer's protocol. A TOPscript^{TM} cDNA synthesis kit (Enzynomics, EZ005S, South Korea) was used to reverse transcribe 1 μg of the extracted RNAs into cDNA. 10 ng of each cDNA sample was analyzed using the StepOnePlus Real-Time System (Thermo Fisher) with Power SYBR Green PCR Master Mix (Thermo Fisher, 4367659, UK). Primers for human *PLIN2* (OCH8054/OCH8055) and *ACTB* (encoding β-actin) (OCH6531/OCH6532) were designed using NCBI Primer-BLAST. The cycles of quantitative real-time PCR are as follow: 95 °C for 10 min, followed by 40 cycles of 95 °C for 15 s and 58 °C for 1 min. The $\Delta\Delta C_T$ method was used to calculate the relative expression levels of *PLIN2*. Table 2 describes the primer sequences of *PLIN2* and *ACTB* in detail.

In vivo ubiquitylation assay

HeLa cells were seeded at 1 × 10^6 cells/10-cm plate in DMEM supplemented with 10% FBS. After a 24-h incubation, cells were co-transfected with pCH5097 (expressing N-terminally HA-tagged Ub), pCH6571 (expressing C-terminally myc-tagged $PLIN2_{myc}$), and pcDNA3.1 (control), pCH879 (expressing C-terminally triply FLAG-tagged $TEB4_{f3}$), or pCH881 (expressing catalytically inactive $TEB4_{f3}{}^{C9A}$). After a 24-h incubation, the transfected cells were treated with 10 μM MG132 for 8 h, harvested via centrifugation at 17,500 × *g* for 15 min, and lysed in TLE buffer (50 mM Tris-HCl, 150 mM NaCl, 1% Nonidet P-40, 1 mM EGTA, 1 mM Na-EDTA, pH 7.5) supplemented with 1× protease inhibitor mixture, 10 mM iodoacetamide, and *N*-ethylmaleimide. $PLIN2_{myc}$ was immunoprecipitated using pre-conjugated rabbit anti-myc antibodies with Dynabeads Protein A (Thermo Fisher Scientific, 10001D) for 3 h at 4 °C. Polyubiquitylated $PLIN2_{myc}$ were eluted using 30 μl of 1× Laemmli sample buffer and fractionated by SDS-10% PAGE, followed by immunoblotting with anti-HA (for ubiquitylated $PLIN2_{myc}$ detection) and anti-myc mouse IgG (for $PLIN2_{myc}$ detection).

Chemical cross-linking and co-immunoprecipitation analyses

For cross-linking/co-immunoprecipitation experiments, HeLa cells (~70% confluence) in 10-cm culture dishes were co-transfected with 3 μg of either pCH879 (expressing TEB_{3f}) or pCH60 and 2 μg of either pCH6567 or pCH6568 (expressing [M]A-$PLIN2_{ha2}$ or [M]P-$PLIN2_{ha2}$, respectively) for co-immunoprecipitation by FLAG using the PEI transfection method. Conversely, for complementary co-IP by HA, HeLa cells (~70% confluence) in 10-cm culture dishes were co-transfected with 2 μg of pCH60, pCH6567, or pCH6568, and 3 μg of pCH879 in the same transfection method as described above. After a 48-h incubation, cells were treated with MG132 at a final concentration of 10 μM for 4 h, and thereafter with 1 mM DSP, a membrane-permeable amino group-specific cross-linking reagent. After a 2-h incubation on ice, the *in vivo* cross-linking reaction was stopped by the addition of 10 mM Tris-HCl (pH 7.5) for 15 min at room temperature to quench unreacted DSP. The cross-linked cells were washed twice in 1× PBS (Lonza, 17-516Q), gently scraped from plates, and pelleted via low-speed centrifugation at 800 × *g* for 5 min at 4 °C. The pelleted cells were lysed by resuspending them in 0.8 ml of lysis buffer (1% Nonidet P-40, 0.15 M NaCl, 1 mM Na-EDTA, 50 mM Tris-HCl, pH 7.5), plus 1× cOmplete protease inhibitor mixture (Roche Applied Science)) and incubating on ice for 20 min. After a brief sonication, the cell extracts were centrifuged at 17,500 × *g* for 20 min at 4 °C. Then, the supernatant was transferred to a tube chilled on ice. To pre-clear the lysates, cell extracts were incubated with 3 μl of IgG Dynabeads (Thermo Fisher Scientific, 10003D) at 4 °C for 30 min. After the pre-clearing step, total protein concentrations in the supernatants were determined using the Bradford assay (Bio-Rad, 5000006) according to the manufacturers' protocols. The cell extracts (1 mg of total proteins) were incubated with anti-HA or anti-FLAG bound IgG Dynabeads at 4 °C for 2 h, and the magnetic beads were washed three times in washing buffer (0.2% Nonidet P-40, 137 mM NaCl, 2 mM Na-EDTA, 10% glycerol, 20 mM Tris-HCl, pH 7.5). The bound proteins were eluted in 45 μl of 2× Laemmli sample buffer and incubated for 20 min at 37 °C, followed by separation using SDS-12% PAGE and immunoblotting with anti-HA or anti-FLAG antibodies.

LD staining and quantification

For LD staining, HeLa cells were seeded at 2 × 10^5 cells onto a poly-L-lysine (Sigma, P4832) treated coverslip in DMEM supplemented with 10% FBS for 24 h. The cells were washed twice in PBS (Lonza, 17-516Q), fixed in 4% paraformaldehyde for 10 min at room temperature, and washed again three times with PBS. The fixed cells were permeabilized with 0.2% Triton X-100 (Sigma, ×100) for 5 min and washed three times with PBS before staining with 1 μM BODIPY 493/503 (Thermo Fisher, D3922) in PBS for 30 min at room temperature. The stained cells were washed three times in PBS and mounted in ProLong^{TM} Gold Antifade Mountant with 4′,6-diamidino-2-phenylindole (Thermo Fisher Scientific, P36941). For LD visualization, *Z*-stack confocal images were obtained with a FLUOVIEW FV3000 laser scanning confocal microscope (OLYMPUS, Japan) using an UPLSAPO ×60/1.35 NA oil objective and a pinhole of 1.0 airy units. Images were taken using a 405-nm laser for 4′,6-diamidino-2-phenylindole detection, and a 488-nm laser for LD detection. Optical *Z*-sections (0.5 μm) were obtained at a speed of 8 μs/pixel by line scan (640 × 640 pixels; 12 bits/pixel) for 3D reconstructions and image analysis. For image analysis and LD quantification, Imaris software CUDA Deconvolution extension (Bitplain, version 9.1.2) was used to conduct 3D deconvolution. LD vesicles were detected on a per-cell basis using the "Cells" tool in Imaris (Bitplain, version 9.1.2) to detect cell boundaries, then vesicle detection wherein the size of the largest sphere was 0.5–1.0 μm (dependent on average LD size for the samples), background subtraction threshold based on LD size, and the built-in "quality" threshold. Cells with no nucleus or on the very edge of an image were excluded from the datasets during analysis.

All LDs were counted on a per-cell basis, >30 cells, and are a representative set of $n \geq 3$ experiments.

Statistical analysis

To evaluate significant differences (p values), two-tailed unpaired Student's t tests were conducted using Microsoft Excel. $p < 0.05$ was considered significantly different. All the values displayed are mean ± S.E. or mean ± S.D. as indicated, which were calculated using Excel. Column scatter plots, which shows the difference in LD number, were performed by GraphPad Prism 6.

Author contributions—K. T. N., C.-S. L., S.-H. M., and C.-S. H. conceptualization; K. T. N., S.-H. M., N. T. T., S. K. P., and C.-S. H. resources; K. T. N., S. K. P., and C. -S. H. data curation; K. T. N., S.-H. M., N. T. T., S. K. P., and C.-S. H. software; K. T. N., C.-S. L., S.-H. M., N. T. T., and C.-S. H. formal analysis; K. T. N., C.-S. L., S.-H. M., N. T. T., S. K. P., and C.-S. H. validation; K. T. N., C.-S. L., S.-H. M., N. T. T., and C.-S. H. investigation; K. T. N., C.-S. L., N. T. T., and C.-S. H. visualization; K. T. N., C.-S. L., S.-H. M., N. T. T., S. K. P., and C.-S. H. methodology; K. T. N., C.-S. L., S.-H. M., and C.-S. H. writing-review and editing; S. K. P. and C.-S. H. supervision; C.-S. H. funding acquisition; C.-S. H. writing-original draft; C.-S. H. project administration.

Acknowledgments—We thank the current and former members of Dr. Hwang's laboratory for assistance and comments on the paper.

References

1. Conte, M., Franceschi, C., Sandri, M., and Salvioli, S. (2016) Perilipin 2 and age-related metabolic diseases: a new perspective. *Trends Endocrinol. Metab.* **27,** 893–903 CrossRef Medline
2. Bersuker, K., and Olzmann, J. A. (2017) Establishing the lipid droplet proteome: mechanisms of lipid droplet protein targeting and degradation. *Biochim. Biophys. Acta* **1862,** 1166–1177 CrossRef
3. Itabe, H., Yamaguchi, T., Nimura, S., and Sasabe, N. (2017) Perilipins: a diversity of intracellular lipid droplet proteins. *Lipids Health Dis.* **16,** 83 CrossRef Medline
4. Kaushik, S., and Cuervo, A. M. (2015) Degradation of lipid droplet-associated proteins by chaperone-mediated autophagy facilitates lipolysis. *Nat. Cell. Biol.* **17,** 759–770 CrossRef Medline
5. Takahashi, Y., Shinoda, A., Kamada, H., Shimizu, M., Inoue, J., and Sato, R. (2016) Perilipin2 plays a positive role in adipocytes during lipolysis by escaping proteasomal degradation. *Sci. Rep.* **6,** 20975 CrossRef Medline
6. Masuda, Y., Itabe, H., Odaki, M., Hama, K., Fujimoto, Y., Mori, M., Sasabe, N., Aoki, J., Arai, H., and Takano, T. (2006) ADRP/adipophilin is degraded through the proteasome-dependent pathway during regression of lipid-storing cells. *J. Lipid Res.* **47,** 87–98 CrossRef Medline
7. Xu, G., Sztalryd, C., Lu, X., Tansey, J. T., Gan, J., Dorward, H., Kimmel, A. R., and Londos, C. (2005) Post-translational regulation of adipose differentiation-related protein by the ubiquitin/proteasome pathway. *J. Biol. Chem.* **280,** 42841–42847 CrossRef Medline
8. Kory, N., Thiam, A. R., Farese, R. V., Jr., and Walther, T. C. (2015) Protein crowding is a determinant of lipid droplet protein composition. *Dev. Cell* **34,** 351–363 CrossRef Medline
9. Varshavsky, A. (2011) The N-end rule pathway and regulation by proteolysis. *Protein Sci.* **20,** 1298–1345 CrossRef Medline
10. Cha-Molstad, H., Yu, J. E., Feng, Z., Lee, S. H., Kim, J. G., Yang, P., Han, B., Sung, K. W., Yoo, Y. D., Hwang, J., McGuire, T., Shim, S. M., Song, H. D., Ganipisetti, S., Wang, N., *et al.* (2017) p62/SQSTM1/Sequestosome-1 is an N-recognin of the N-end rule pathway which modulates autophagosome biogenesis. *Nat. Commun.* **8,** 102 CrossRef Medline
11. Lee, K. E., Heo, J. E., Kim, J. M., and Hwang, C. S. (2016) N-terminal acetylation-targeted N-end rule proteolytic system: the Ac/N-end rule pathway. *Mol. Cells* **39,** 169–178 CrossRef Medline
12. Nguyen, K. T., Mun, S. H., Lee, C. S., and Hwang, C. S. (2018) Control of protein degradation by N-terminal acetylation and the N-end rule pathway. *Exp. Mol. Med.* **50,** 91 CrossRef Medline
13. Dissmeyer, N., Rivas, S., and Graciet, E. (2018) Life and death of proteins after protease cleavage: protein degradation by the N-end rule pathway. *New Phytol.* **218,** 929–935 CrossRef Medline
14. Kim, H. K., Kim, R. R., Oh, J. H., Cho, H., Varshavsky, A., and Hwang, C. S. (2014) The N-terminal methionine of cellular proteins as a degradation signal. *Cell* **156,** 158–169 CrossRef Medline
15. Chen, S. J., Wu, X., Wadas, B., Oh, J. H., and Varshavsky, A. (2017) An N-end rule pathway that recognizes proline and destroys gluconeogenic enzymes. *Science* **355,** eaal3655 CrossRef Medline
16. Hwang, C. S., Shemorry, A., and Varshavsky, A. (2010) N-terminal acetylation of cellular proteins creates specific degradation signals. *Science* **327,** 973–977 CrossRef Medline
17. Shemorry, A., Hwang, C. S., and Varshavsky, A. (2013) Control of protein quality and stoichiometries by N-terminal acetylation and the N-end rule pathway. *Mol. Cell* **50,** 540–551 CrossRef Medline
18. Park, S. E., Kim, J. M., Seok, O. H., Cho, H., Wadas, B., Kim, S. Y., Varshavsky, A., and Hwang, C. S. (2015) Control of mammalian G protein signaling by N-terminal acetylation and the N-end rule pathway. *Science* **347,** 1249–1252 CrossRef Medline
19. Wadas, B., Borjigin, J., Huang, Z., Oh, J. H., Hwang, C. S., and Varshavsky, A. (2016) Degradation of serotonin *N*-acetyltransferase, a circadian regulator, by the N-end rule pathway. *J. Biol. Chem.* **291,** 17178–17196 CrossRef Medline
20. Xu, F., Huang, Y., Li, L., Gannon, P., Linster, E., Huber, M., Kapos, P., Bienvenut, W., Polevoda, B., Meinnel, T., Hell, R., Giglione, C., Zhang, Y., Wirtz, M., Chen, S., and Li, X. (2015) Two N-terminal acetyltransferases antagonistically regulate the stability of a nod-like receptor in *Arabidopsis*. *Plant Cell* **27,** 1547–1562 CrossRef Medline
21. Xiao, Q., Zhang, F., Nacev, B. A., Liu, J. O., and Pei, D. (2010) Protein N-terminal processing: substrate specificity of *Escherichia coli* and human methionine aminopeptidases. *Biochemistry* **49,** 5588–5599 CrossRef Medline
22. Bienvenut, W. V., Sumpton, D., Martinez, A., Lilla, S., Espagne, C., Meinnel, T., and Giglione, C. (2012) Comparative large scale characterization of plant *versus* mammal proteins reveals similar and idiosyncratic *N*-α-acetylation features. *Mol. Cell. Proteomics* **11,** M111.015131 Medline
23. Van Damme, P., Lasa, M., Polevoda, B., Gazquez, C., Elosegui-Artola, A., Kim, D. S., De Juan-Pardo, E., Demeyer, K., Hole, K., Larrea, E., Timmerman, E., Prieto, J., Arnesen, T., Sherman, F., Gevaert, K., and Aldabe, R. (2012) N-terminal acetylome analyses and functional insights of the N-terminal acetyltransferase NatB. *Proc. Natl. Acad. Sci. U.S.A.* **109,** 12449–12454 CrossRef Medline
24. Ree, R., Varland, S., and Arnesen, T. (2018) Spotlight on protein N-terminal acetylation. *Exp. Mol. Med.* **50,** 90 CrossRef Medline
25. Aksnes, H., Hole, K., and Arnesen, T. (2015) Molecular, cellular, and physiological significance of N-terminal acetylation. *Int. Rev. Cell Mol. Biol.* **316,** 267–305 CrossRef Medline
26. Turner, G. C., and Varshavsky, A. (2000) Detecting and measuring cotranslational protein degradation *in vivo*. *Science* **289,** 2117–2120 CrossRef Medline
27. Qian, S. B., Princiotta, M. F., Bennink, J. R., and Yewdell, J. W. (2006) Characterization of rapidly degraded polypeptides in mammalian cells reveals a novel layer of nascent protein quality control. *J. Biol. Chem.* **281,** 392–400 CrossRef Medline
28. Schubert, U., Antón, L. C., Gibbs, J., Norbury, C. C., Yewdell, J. W., and Bennink, J. R. (2000) Rapid degradation of a large fraction of newly synthesized proteins by proteasomes. *Nature* **404,** 770–774 CrossRef Medline
29. Hassink, G., Kikkert, M., van Voorden, S., Lee, S. J., Spaapen, R., van Laar, T., Coleman, C. S., Bartee, E., Früh, K., Chau, V., and Wiertz, E. (2005) TEB4 is a C4HC3 RING finger-containing ubiquitin ligase of the endoplasmic reticulum. *Biochem. J.* **388,** 647–655 CrossRef Medline

30. Johnsson, N., and Varshavsky, A. (1994) Split ubiquitin as a sensor of protein interactions *in vivo*. *Proc. Natl. Acad. Sci. U.S.A.* **91,** 10340–10344 CrossRef Medline
31. Möckli, N., Deplazes, A., Hassa, P. O., Zhang, Z., Peter, M., Hottiger, M. O., Stagljar, I., and Auerbach, D. (2007) Yeast split-ubiquitin-based cytosolic screening system to detect interactions between transcriptionally active proteins. *BioTechniques* **42,** 725–730 CrossRef Medline
32. Aksnes, H., Drazic, A., Marie, M., and Arnesen, T. (2016) First things first: vital protein marks by N-terminal acetyltransferases. *Trends Biochem. Sci.* **41,** 746–760 CrossRef Medline
33. Goetze, S., Qeli, E., Mosimann, C., Staes, A., Gerrits, B., Roschitzki, B., Mohanty, S., Niederer, E. M., Laczko, E., Timmerman, E., Lange, V., Hafen, E., Aebersold, R., Vandekerckhove, J., Basler, K., Ahrens, C. H., Gevaert, K., and Brunner, E. (2009) Identification and functional characterization of N-terminally acetylated proteins in *Drosophila melanogaster*. *PLos Biol.* **7,** e1000236 CrossRef Medline
34. Carr, R. M., Peralta, G., Yin, X., and Ahima, R. S. (2014) Absence of perilipin 2 prevents hepatic steatosis, glucose intolerance and ceramide accumulation in alcohol-fed mice. *PLoS ONE* **9,** e97118 CrossRef Medline
35. Imamura, M., Inoguchi, T., Ikuyama, S., Taniguchi, S., Kobayashi, K., Nakashima, N., and Nawata, H. (2002) ADRP stimulates lipid accumulation and lipid droplet formation in murine fibroblasts. *Am. J. Physiol. Endocrinol. Metab.* **283,** E775–E783 CrossRef Medline
36. Gao, J., and Serrero, G. (1999) Adipose differentiation related protein (ADRP) expressed in transfected COS-7 cells selectively stimulates long chain fatty acid uptake. *J. Biol. Chem.* **274,** 16825–16830 CrossRef Medline
37. Xu, G., Sztalryd, C., and Londos, C. (2006) Degradation of perilipin is mediated through ubiquitination-proteasome pathway. *Biochim. Biophys. Acta* **1761,** 83–90 CrossRef Medline
38. Senthivinayagam, S., McIntosh, A. L., Moon, K. C., and Atshaves, B. P. (2013) Plin2 inhibits cellular glucose uptake through interactions with SNAP23, a SNARE complex protein. *PLoS ONE* **8,** e73696 CrossRef Medline
39. Ruggiano, A., Mora, G., Buxó, L., and Carvalho, P. (2016) Spatial control of lipid droplet proteins by the ERAD ubiquitin ligase Doa10. *EMBO J.* **35,** 1644–1655 CrossRef Medline
40. Kats, I., Khmelinskii, A., Kschonsak, M., Huber, F., Knieß, R. A., Bartosik, A., and Knop, M. (2018) Mapping degradation signals and pathways in a eukaryotic N-terminome. *Mol. Cell* **70,** 488–501.e485 CrossRef Medline
41. Helbig, A. O., Gauci, S., Raijmakers, R., van Breukelen, B., Slijper, M., Mohammed, S., and Heck, A. J. (2010) Profiling of *N*-acetylated protein termini provides in-depth insights into the N-terminal nature of the proteome. *Mol. Cell. Proteomics* **9,** 928–939 CrossRef Medline
42. Yeom, J., Ju, S., Choi, Y., Paek, E., and Lee, C. (2017) Comprehensive analysis of human protein N-termini enables assessment of various protein forms. *Sci. Rep.* **7,** 6599 CrossRef Medline
43. Zelcer, N., Sharpe, L. J., Loregger, A., Kristiana, I., Cook, E. C., Phan, L., Stevenson, J., and Brown, A. J. (2014) The E3 ubiquitin ligase MARCH6 degrades squalene monooxygenase and affects 3-hydroxy-3-methyl-glutaryl coenzyme A reductase and the cholesterol synthesis pathway. *Mol. Cell. Biol.* **34,** 1262–1270 CrossRef Medline
44. Loregger, A., Cook, E. C., Nelson, J. K., Moeton, M., Sharpe, L. J., Engberg, S., Karimova, M., Lambert, G., Brown, A. J., and Zelcer, N. (2016) A MARCH6 and IDOL E3 ubiquitin ligase circuit uncouples cholesterol synthesis from lipoprotein uptake in hepatocytes. *Mol. Cell. Biol.* **36,** 285–294 Medline
45. Mashiko, D., Fujihara, Y., Satouh, Y., Miyata, H., Isotani, A., and Ikawa, M. (2013) Generation of mutant mice by pronuclear injection of circular plasmid expressing Cas9 and single guided RNA. *Sci. Rep.* **3,** 3355 CrossRef Medline
46. Foresti, O., Ruggiano, A., Hannibal-Bach, H. K., Ejsing, C. S., and Carvalho, P. (2013) Sterol homeostasis requires regulated degradation of squalene monooxygenase by the ubiquitin ligase Doa10/Teb4. *Elife* **2,** e00953 CrossRef Medline
47. Sherman, F. (1991) Getting started with yeast. *Methods Enzymol.* **194,** 3–21 CrossRef Medline
48. Janke, C., Magiera, M. M., Rathfelder, N., Taxis, C., Reber, S., Maekawa, H., Moreno-Borchart, A., Doenges, G., Schwob, E., Schiebel, E., and Knop, M. (2004) A versatile toolbox for PCR-based tagging of yeast genes: new fluorescent proteins, more markers and promoter substitution cassettes. *Yeast* **21,** 947–962 CrossRef Medline
49. Cong, L., Ran, F. A., Cox, D., Lin, S., Barretto, R., Habib, N., Hsu, P. D., Wu, X., Jiang, W., Marraffini, L. A., and Zhang, F. (2013) Multiplex genome engineering using CRISPR/Cas systems. *Science* **339,** 819–823 CrossRef Medline